materials

MDPI

Article

Fabrication and Optical Characterization of VO_2-Based Thin Films Deposited on Practical Float Glass by Magnetron Sputtering and Professional Annealing

Xinhong Chu [1,*], Qiusheng Xie [1], Xiaoming Zhang [1], Bingfeng Guo [1], Jianqing Liao [1] and Xiujian Zhao [2,*]

[1] College of Physics Science and Engineering Technology, Yichun University, Yichun 336000, China; lr@jxycu.edu.cn (Q.X.); zhangxm@jxycu.edu.cn (X.Z.); guobingfeng@jxycu.edu.cn (B.G.); jq-liao@jxycu.edu.cn (J.L.)

[2] State Key Laboratory of Silicate Materials for Architectures, Wuhan University of Technology, Wuhan 430070, China

* Correspondence: cxh@jxycu.edu.cn (X.C.); opluse@whut.edu.cn (X.Z.)

Abstract: In this paper, VO_2 thin films with good optical properties are fabricated on practical float glass by magnetron sputtering and a professional annealing method. The near-infrared switching efficiency (NIRSE) of the prepared film reaches 39% (@2000 nm), and its near-infrared energy modulation ability (ΔT_{ir}) reaches 10.9% (780–2500 nm). Further, the highest integral visible transmittance T_{lum} is 63%. The proposed method exhibits good reproducibility and does not cause any heat damage to the magnetron sputtering machine. The crystalline structure of the VO_2 film is characterized by X-ray diffraction (XRD). The lattice planes (011) and (−211) grow preferentially (JCPDS 65-2358), and a large number of NaV_2O_5 crystals are detected simultaneously. The microstructures are characterized by scanning electron microscopy (SEM), and a large number of long sheet crystals are identified. The phase transition temperature is significantly reduced by an appropriate W doping concentration (T_c = 29 °C), whereas excessive W doping causes distortion of the thermal hysteresis loop and a reduction in the NIRSE. Oxygen vacancies are created by low pressure annealing, due to which the phase transition temperature of VO_2 film decreases by 8 °C. The addition of an intermediate SiO_2 layer can prevent the diffusion of Na^+ ions and affect the preparation process of the VO_2 thin film.

Keywords: VO_2; sputtering; annealing; float glass; W doping; oxygen vacancy; Na^+ ions

Citation: Chu, X.; Xie, Q.; Zhang, X.; Guo, B.; Liao, J.; Zhao, X. Fabrication and Optical Characterization of VO_2-Based Thin Films Deposited on Practical Float Glass by Magnetron Sputtering and Professional Annealing. *Materials* **2022**, *15*, 2990. https://doi.org/10.3390/ma15092990

Academic Editor: Bogdana Mitu

Received: 15 March 2022
Accepted: 18 April 2022
Published: 20 April 2022

1. Introduction

Vanadium dioxide is a typical thermochromic smart material, which was discovered by Morin in 1959 [1]. Below 68 °C, it is a monoclinic semiconductor, while above 68 °C, it becomes a tetragonal conductor. Near the critical point, the electrical and optical properties of VO_2 change by 2–5 orders of magnitude, and the infrared transmittance can change by 40–60% [1–4]. Therefore, VO_2 has garnered considerable research attention for preparing smart windows [5,6], optical switches [7], biomedical sensors [8], relaxation oscillator [9], and so on.

Magnetron sputtering [10,11], chemical vapor deposition (CVD) [12], sol-gel processing [4,13], pulsed laser deposition [14], and molecular beam epitaxy [15] are often used to prepare VO_2 films. Among these methods, magnetron sputtering is the most widely used method owing to its advantages of controllable film thickness, high speed, low temperature, good adhesion, high production efficiency, environmental friendliness, and great industrial potential, and it can be used to prepare compact, homogeneous, and stable films. However, it faces the problems of complex process, difficult operation, and poor reproducibility in preparing VO_2 thin films. Therefore, Gurvitch et al. [16] and Luo et al. [17] firstly used magnetron sputtering to prepare metal V film and then utilized in situ oxidative annealing to prepare VO_2 thin films, which exhibited good repeatability. However, the in-situ annealing

operation at high temperature (above 300–500 °C) can damage the magnetron sputtering equipment and shorten its working life. Liu et al. [18], Xu et al. [19], and Ba et al. [20] deposited V metal films on glass and sapphire by magnetron sputtering or ion-assisted sputtering technology and then obtained VO_2 films by oxidative annealing in pure oxygen atmosphere or air atmosphere in a furnace. This two-step technique was beneficial to improve the reproducibility and protect the sputtering equipment, but they did no further works in studies of substrates, visible transmittance improvement, doping, oxygen vacancies, and so on. Silicon [21], quartz [10,22], sapphire [10,23], and other materials are often used as substrates for depositing VO_2 film to achieve better phase transition performance. However, these substrates are expensive, difficult to obtain, and inconsistent with the actual glass used in windows and doors. Float glass (Na-Ca-Si ternary glass, Na~13.8%, Ca~8.6%, Si~72.8%, others~4.8%) is the most widely used practical glass in modern buildings, so it must be explored as a substrate for VO_2 to be applied in smart windows. Presently, the most vital problem of float glass is that small Na^+ ions can easily diffuse into the VO_2 film, which results in poor thermochromic properties [24]. VO_2 thin films have been prepared on Si_3N_4 [25], TiO_2 [26], ZnO [27], SnO_2 [28], and other buffer layers, but the preparation methods and properties were quite different. For application in smart windows, the VO_2 film's visible transmittance should be above 60%, and the key performance of the transition temperature must be reduced to a practical range of 25–30 °C. Tungsten doping and oxygen vacancy production have been considered to be effective methods [29–31], but the mechanisms of tungsten doping for reducing the phase transition temperature and the equivalent effect of oxygen vacancy are still not clear.

In this study, a two-step method of magnetron sputtering and professional annealing with good reproducibility and no heat damage to the sputtering machine was successfully utilized to deposit VO_2-based thermochromic thin films on a practical float glass, including intrinsic VO_2 thin films, VO_2 thin films with intermediate SiO_2 layers, and W-doped VO_2 thin films. Further, the annealing control, visible transmittance adjustment, the effect of 100-nm-thick intermediate SiO_2 layer on preventing the diffusion of Na^+ ions, and the equivalent action of W dopant and O vacancy were investigated.

2. Materials and Methods

2.1. Preparation of V-Based Metal Films by Magnetron Sputtering

The practical float glass used in this study was SAIL BRAND 7101 with a thickness of 1 mm. The magnetron sputtering machine used was ADV-ZKS-0350 (Aitmet Vacuum Machinery Co., Ltd., Foshan, Guangdong, China). The float glass (hereafter referred to as glass) was cut into a size of 25.4 mm × 38.1 mm, then ultrasonically cleaned in acetone and anhydrous ethanol for 30 min, and subsequently dried off for later use. The sputtering vacuum chamber was thoroughly cleaned, and then the V metal target (φ: 56 mm, 99.9% purity) and glass substrate were installed. The chamber was vacuumized to 3.0×10^{-3} Pa, and then Ar gas (99.99% purity) was passed through it to achieve a pressure of 1 Pa. DC magnetron sputtering was utilized to deposit the V-based metal films at room temperature (20 °C). The impurity atoms on the target surface were removed by pre-sputtering for 10 min, and then the baffle was opened to deposit films at a power of 77 W. The sputtering time was controlled to 5, 7.5, and 10 min to obtain V metal films with thicknesses of 30, 45, and 60 nm (calculated by statistical average deposition rate), respectively. The main process parameters are shown in Table 1, and the quartz glass is a contrast substrate.

Table 1. Preparation parameters of V-based metal films by magnetron sputtering.

Substrate	Target	Background Pressure (Pa)	Working Gas	Working Pressure (Pa)	Substrate Temperature (°C)	Sputtering Method	Power (W)	Sputtering Time (min)	V Film Thickness (nm)
Glass	V	3.0×10^{-3}	Ar	1	20	DC	77	5, 7.5, 10	30, 45, 60
Quartz glass	V	3.0×10^{-3}	Ar	1	20	DC	77	5	30
SiO_2 (/glass)	V	3.0×10^{-3}	Ar	1	20	DC	77	5	30
Glass	W/V	3.0×10^{-3}	Ar	1	20	DC	77	7.5	45

W/V inlaid target (φ: 56 mm, W purity: 99.95%, V purity: 99.9%, Figure 1) and DC magnetron sputtering technology were applied to execute W doping in an appropriate ratio (0–1.0%, the ratio of the area of W bars to the total area of the target). According to the sputtering yield, sputtering area, and atomic concentration, the W dopant ratio by mol can be calculated according to the area ratio of W bars. The W dopant's ratios by area of 0%, 0.5%, and 1% correspond to the ratios by mol of 0%, 2.83%, and 5.53%, respectively. For convenience, the W dopant ratio in this paper represents the area ratio unless otherwise specified. The sputtering time for the W:V metal film was 7.5 min, and the thickness was approximately 45 nm. The main process parameters are shown in Table 1.

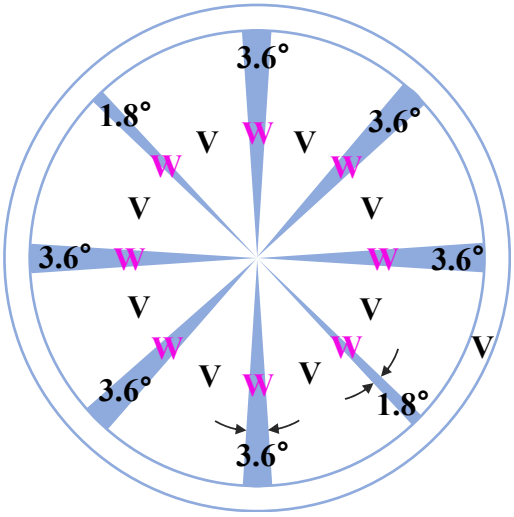

Figure 1. Schematic of the tungsten-vanadium inlaid target (when W bars are fully embedded, doping ratio-max: 7%). (The blue bar is W. One 1.8° W bar represents 0.5% doping ratio by area, and one 3.6° W bar represents 1.0% doping ratio by area; Increase the number of W bars can get different W doping concentrations, and the maximum can reach 7%).

RF magnetron sputtering technology was used to deposit the SiO_2 layer on the glass for blocking the sodium ion diffusion. The main process parameters are shown in Table 2. Then, 30 nm V metal film was spread on the intermediate SiO_2 layer (Table 1).

Table 2. Preparation parameters of the intermediate SiO_2 layer by RF magnetron sputtering.

Substrate	Target	Background Pressure (Pa)	Working Pressure (Pa, Ar)	Substrate Temperature (°C)	Sputtering Method	Power (W)	Sputtering Time (min)	SiO_2 Film Thickness (nm)
Glass	SiO_2	3.0×10^{-3}	1	200	RF	100	50	100

2.2. Preparation of VO_2-Based Films by Professional Annealing

The deposited V-based metal films (V, W:V, V/SiO_2) were placed in a vacuum tube furnace (ECFK-6-14), vacuumized to a needed low pressure, heated to 400 °C at 5 °C/min, annealed in low pressure air atmosphere for 1 h, and then naturally cooled to room temperature to obtain VO_2-based films. The main process parameters are shown in Table 3, and the quartz glass is a contrast substrate.

Table 3. Preparation parameters of VO_2-based films by professional annealing.

Metal Film/Substrate	Annealing Atmosphere	Background Pressure (Pa)	Annealing Temperature (°C)	Heating Rate (°C/min)	Annealing Time (h)
30 nm V/glass	air	50, 100, 200, 450, 1500	400	5	1
45 nm V/glass	air	200, 450, 700	400	5	1
60 nm V/glass	air	450	400	5	1
30 nm V/quartz glass	air	1500	400	5	1
30 nm V/SiO_2/glass	air	200, 450, 600	400	5	1
45 nm W:V/glass	air	300, 450	400	5	1

2.3. Testing and Characterization

The transmittance of the film was examined using ultraviolet-visible-infrared spectrophotometry (UV-3600 MPC 3100, Shimadsu, Kyoto, Japan), where the testing wavelength range was 250–2500 nm, the step length was 1 nm, and the testing temperature was 20 and 90 °C. The heating attachment was a small numerical control furnace with a temperature error of ±1 °C. The near-infrared switching efficiency (NIRSE) is defined as the difference between the transmittance at low temperature and the transmittance at high temperature at 2000 nm. The thermal hysteresis loop was drawn using the transmittance curves at different temperatures in the range of 20–90 °C with an interval of 5 °C both in the heating and cooling process. Further, each temperature point was held for at least 5 min before obtaining the transmittance curve. Moreover, a standard VO_2 film sample (quartz glass substrate, NIRSE 50%, i.e., the VO_2 film by "30 nm V/quartz glass" in Table 3) was used to complete the transmittance measurement in whole wavelength 250–2500 nm at any two temperature points, e.g., 20 °C and 40 °C, to check the sameness and uniformity of the transmittance curve before every loop test. To obtain the thermal hysteresis loop of the VO_2 film, the transmittance values at 2000 nm in each curve were considered as the *Y*-axis, and temperature points were taken for the *X*-axis.

The phase composition of the as-prepared VO_2-based films were analyzed by X-ray diffraction (XRD; PANalytical Empyrean, PANalytical B.V., Almelo, Netherlands; Cu target, λ = 1.540598 Å, acceleration voltage = 40 kV, and current = 10 mA). The micro morphologies of these films were investigated by field emission scanning electron microscopy (FESEM; Hitachi S-4800, Hitachi, Tokyo, Japan). The oxygen vacancies of related films were investigated by X-ray photoelectron spectroscopy (XPS; VG Mutilab 2000, Thermo Electron Co., Bedford, MA, USA; Al Kα, hν = 1486.6 eV, resolution 0.47 eV).

2.4. Data Treatment

According to the transmittance curve and Equation (1), the visible spectral transmittance can be obtained [32], which is also known as the integrated visual photopic transmission (IVPT, denoted by T_{lum}). This kind of transmittance takes the people's visual perception into account and is more suitable for the daylighting evaluation of green buildings. It is calculated as follows:

$$T_{lum} = \frac{\int_{380}^{780} D_\lambda V(\lambda) T(\lambda) d\lambda}{\int_{380}^{780} D_\lambda V(\lambda) d\lambda} \quad (1)$$

where D_λ is the relative spectral distribution of illuminant D65, $V(\lambda)$ is the spectral luminous efficiency for photopic vision, and $T(\lambda)$ is the visible transmittance. Further, the values of $D_\lambda \cdot V(\lambda) \cdot \Delta\lambda$ were obtained from the international standard ISO 9095-2003.

According to the transmission curve and Equation (2), the near-infrared spectral transmittance (T_{ir}) can be calculated [32]. The regulation ability to near-infrared light (ΔT_{ir}) is expressed as the difference between T_{ir} at high temperature and T_{ir} at low temperature. T_{ir} is calculated as follows:

$$T_{ir} = \frac{\int_{780}^{2500} S_\lambda T(\lambda) d\lambda}{\int_{780}^{2500} S_\lambda d\lambda} \quad (2)$$

where S_λ is the relative spectral distribution of solar radiation, $T(\lambda)$ is the near-infrared transmittance, and the values of $S_\lambda \cdot \Delta\lambda$ were obtained from the international standard ISO 9095-2003.

3. Results

3.1. Transmittance and Microstructure of VO_2 Film Based on the Optimization of Thickness and Pressure

Figure 2a shows that at the annealing pressure of 450 Pa, the NIRSE (39%) of the VO_2 film prepared by the 45 nm V metal film is higher than that prepared by the 30 nm, 60 nm V metal films (20%, 26%). This indicates that the optimal thickness of the V film under this condition is nearly 45 nm. Furthermore, Figure 2b shows that for the 45 nm V metal film, the NIRSE (39%) of VO_2 film prepared at the annealing pressure of 450 Pa is higher than that at 200 and 700 Pa (16%, 30%). This suggests that the optimal annealing pressure of the V film under this condition is approximately 450 Pa. When the thickness and annealing pressure of the VO_2 film are optimized, the NIRSE is enhanced, and the values of $\triangle T_{ir}$ and T_{lum} change accordingly. Generally, as NIRSE increases, ΔT_{ir} increases. When the thickness of the V metal film decreases or the annealing pressure increases, T_{lum} increases, and vice versa, as illustrated in Table 4.

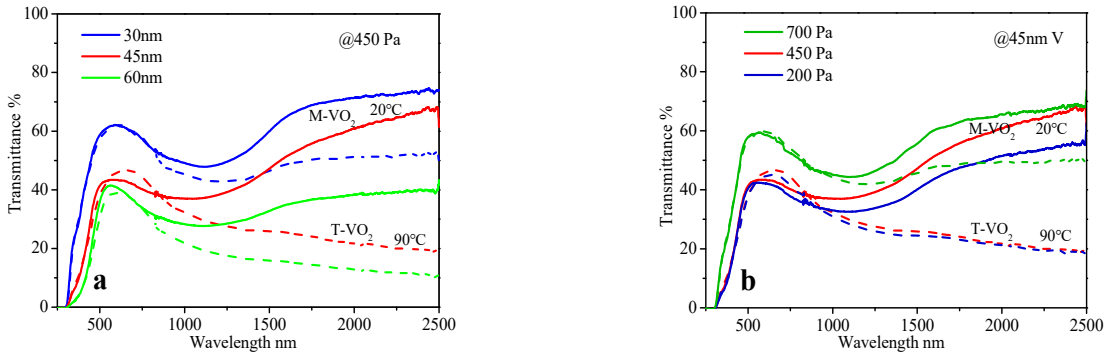

Figure 2. (**a**) Transmittance of VO_2 films prepared by professional annealing of V metal films with different thicknesses at 450 Pa. (**b**) Transmittance of VO_2 films prepared by professional annealing of 45 nm V films at different pressures; all at 400 °C for 1 h; solid line: 20 °C (monoclinic M-VO_2), dashed line: 90 °C (tetragonal T-VO_2).

Table 4. Optical properties of VO_2 thin films prepared by professional annealing under optimized thickness and pressure.

V Film Thickness (nm)-Annealing Pressure (Pa)	NIRSE (@2000 nm)	ΔT_{ir} (780–2500 nm)	T_{lum} (20 °C)	T_{lum} (90 °C)	T_{lum} (Average)
30–450	20%	7.0%	63%	63%	63%
45–450	39%	10.9%	44%	45%	44.5%
60–450	26%	10.1%	41%	38%	39.5%
45–200	16%	7.4%	43%	44%	43.5%
45–700	30%	4.2%	61%	61%	61%

The XRD pattern in Figure 3a shows that the phase composition of VO_2 films prepared by annealing of 30, 45, and 60 nm V film at 450 Pa. With the thickness increasing of V film, the concentration ratio of NaV_2O_5: VO_2 decreases. Because of the low concentration and micro size of the VO_2 particles, the VO_2 film from 30 nm V presents nearly no corresponding diffraction peaks. The VO_2 film prepared by annealing of 45 and 60 nm V film at 450 Pa includes not only a VO_2, but also a NaV_2O_5 diffraction peak. The (011) and (−211) lattice planes of VO_2 grow preferentially, and their diffraction peaks are stronger. The crystalline phase (M, monoclinic) of the VO_2 film corresponds to the standard card JCPDS 65-2358. Moreover, the particle sizes of the VO_2 films by 45 and 60 nm V are both about 15 nm, as calculated by Scherrer formula. The SEM image in Figure 3b suggests that the microstructure of VO_2 films prepared by annealing of 30, 45, and 60 nm V film at 450 Pa is more or less the same. Take the VO_2 film from 45 nm V for instance, where the microstructure is composed of long sheet crystals (length: 210 nm, width: 50 nm, thickness: 20 nm). It can be inferred that the long sheets are NaV_2O_5 crystals, which present obvious oriented growth. The same morphology of NaV_2O_5 crystals was reported by Mjejri et al. [33]. Smaller VO_2 crystalline particles are scattered in the interspace of NaV_2O_5 crystals, which are difficult to observe due to the influence of the depth of field of the long sheet NaV_2O_5 crystals.

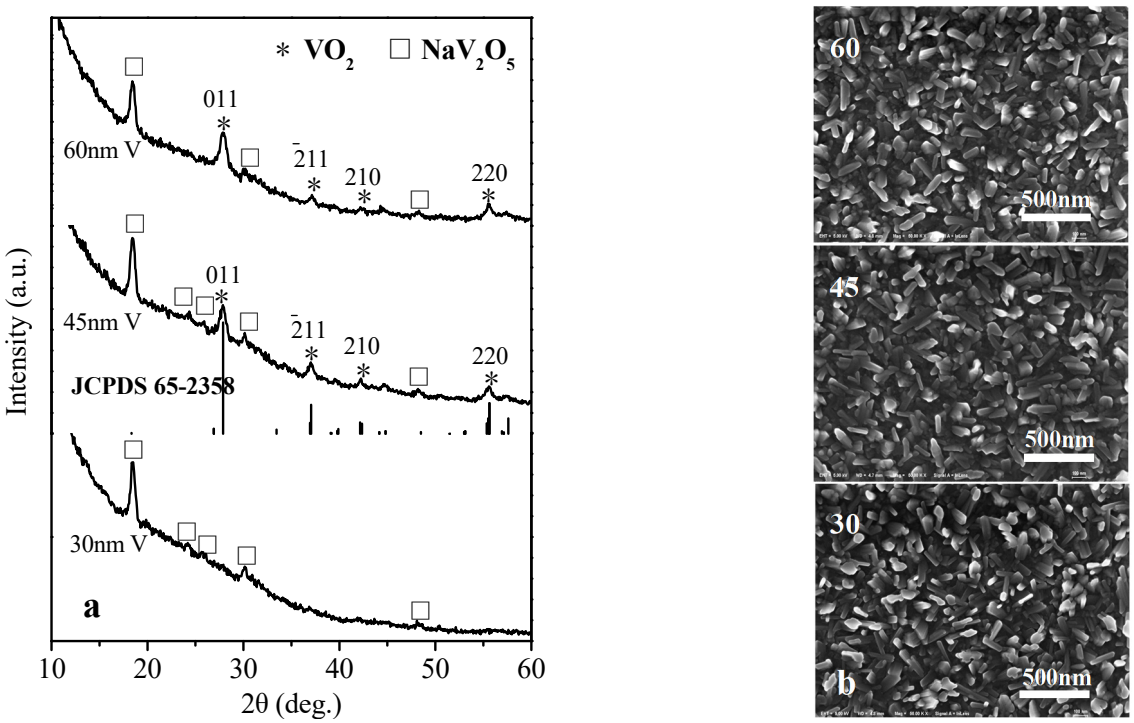

Figure 3. XRD patterns (**a**) and SEM images (**b**) of the VO_2 thin films prepared by professional annealing of the 30, 45, 60 nm V metal films at 450 Pa, 400 °C for 1 h.

The XRD pattern in Figure 4a shows the phase composition of VO_2 films prepared by the annealing of 45 nm V film at pressures 200, 450, 700 Pa. Compared to 200 Pa, the 450 and 700 Pa result in an obvious higher concentration of NaV_2O_5, and the 450 Pa leads to a higher ratio of VO_2: NaV_2O_5 than the 700 Pa. Moreover, the VO_2 film by 450 Pa performs crystalline phase (M) corresponding to the standard card JCPDS 65-2358. And the particle sizes of the VO_2 films by 45 nm V at pressures 200, 450, and 700 Pa are about 12, 15, and 11 nm respectively, calculated by the Scherrer formula. The SEM image in Figure 4b suggests that the microstructures of VO_2 films prepared by the annealing of 45 nm V film at pressures 200, 450, and 700 Pa are quite different. With the pressure increasing, the film microstructure presents bigger and bigger single crystals with an obvious oriented growth and a long sheet morphology, which are inferred to be NaV_2O_5 likewise. VO_2 crystalline particles are scattered in the single crystals with depth of field and are difficult to observe.

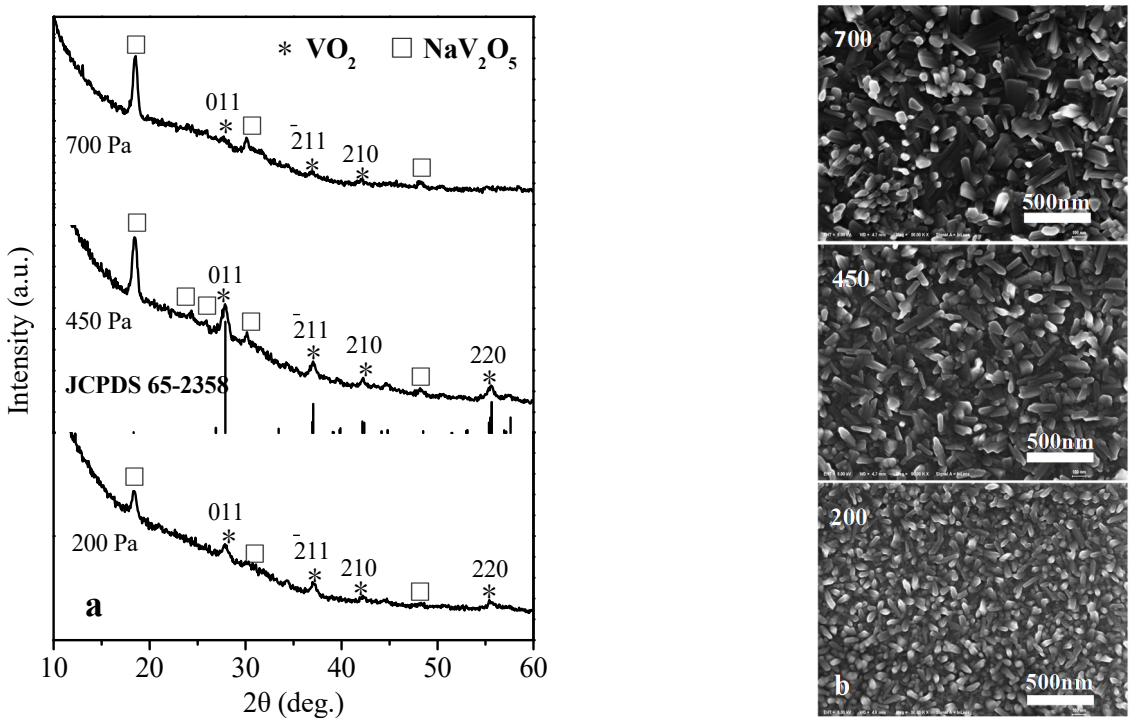

Figure 4. XRD patterns (**a**) and SEM images (**b**) of the VO_2 thin films prepared by professional annealing of 45 nm V films at 200, 450, 700 Pa respectively, 400 °C for 1 h.

When the thickness of V film is reduced from 45 nm to 30 nm, the optimal annealing pressure is reduced to 100 Pa, as shown in Figure 5. In general, thicker V metal films require higher optimal annealing pressure to obtain large NIRSE, and thinner V metal films require lower optimal annealing pressure to obtain large NIRSE. The optical properties of the reduced VO_2 thin films are shown in Table 5.

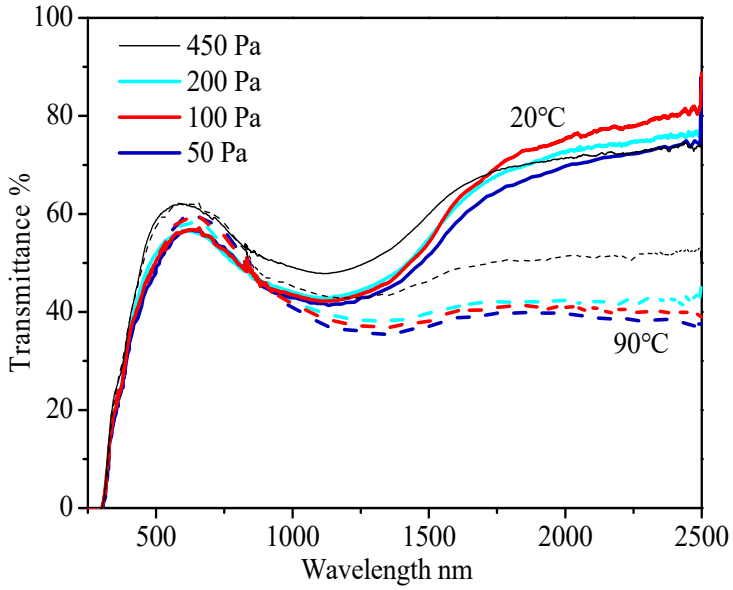

Figure 5. Transmittance of thinner VO_2 films prepared by professional annealing of 30 nm V metal films at different pressures, 400 °C for 1 h; solid line: 20 °C, dashed line: 90 °C.

Table 5. Optical properties of thin VO_2 films prepared by 30 nm V metal films at different annealing pressures.

Annealing Pressure (Pa)	NIRSE (@2000 nm)	ΔT_{ir} (780–2500 nm)	T_{lum} (20 °C)	T_{lum} (90 °C)	T_{lum} (Average)
450	20%	7.0%	63%	63%	63%
200	30%	7.2%	57%	57%	57%
100	35%	8.0%	56%	58%	57%
50	30%	7.3%	55%	57%	56%

3.2. Transmittance, Loops and Microstructure of W-Doped VO_2 Thin Films

According to the transmittance curves in Figure 6a and the thermal hysteresis loops in Figure 6b of the W-doped VO_2 films by 45 nm W:V at 450 Pa, the phase transition temperature (T_c) of 0.5%W-doped VO_2 thin film is significantly decreased (T_c = 29 °C). However, the NIRSE remains high (27%), and the shape of the thermal hysteresis loop is not distorted seriously. With the increase in the concentration of W dopant to 1% (i.e., 1.0%W-doped VO_2 film), the phase transition temperature does not decline continuously but rises, especially above the temperature T_d or $T_{d'}$ (33 °C or 28 °C), due to which the average T_c decreases to 39 °C. In addition, the NIRSE is negatively affected and reduces to 13%. At the same time, the shape of the thermal hysteresis loop is seriously distorted: the height decreases (13%, while for 0.5%W: 27%), the gradient becomes more gentle, and the width increases considerably (16 °C, while for 0.5%W: 7 °C).

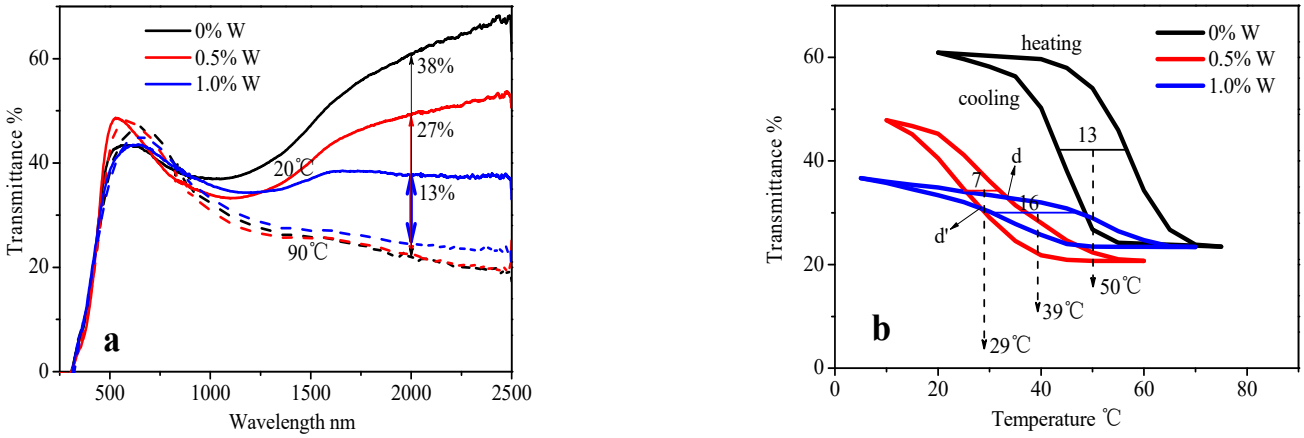

Figure 6. Transmittance curves (**a**) and thermal hysteresis loops (**b**) of VO_2 films with different W doping concentrations prepared by professional annealing of 45 nm W:V films at 450 Pa, 400 °C for 1 h; solid line: 20 °C, dashed line: 90 °C in (**a**).

The XRD pattern in Figure 7a shows that the peak intensities of the crystal NaV_2O_5 and the crystalline VO_2 both decrease with the increase of W dopant. The SEM image in Figure 7b suggests that the size of the long sheet NaV_2O_5 crystal declines gradually with the increase of W dopant, which corresponds to the result of XRD. The W-doped VO_2 crystallites cannot be seen in the SEM image for the depth of field of the long sheet NaV_2O_5 crystals, but the particle size calculated from XRD pattern by the Scherrer formula presents a decline trend too, with 15, 13, and 11 nm, corresponding to 0%, 0.5%, and 1.0%W respectively. W doping makes local T-VO_2 phase increase and M-VO_2 phase decrease, which results in tighter lattice structure and greater difficulty for Na diffusion into the film. In addition, W atom has more free electrons, which leads to a greater reducibility of the doped V film and higher consumption of oxygen. In conclusion, the above two reasons result in the decrement of the crystal NaV_2O_5 and the crystalline VO_2.

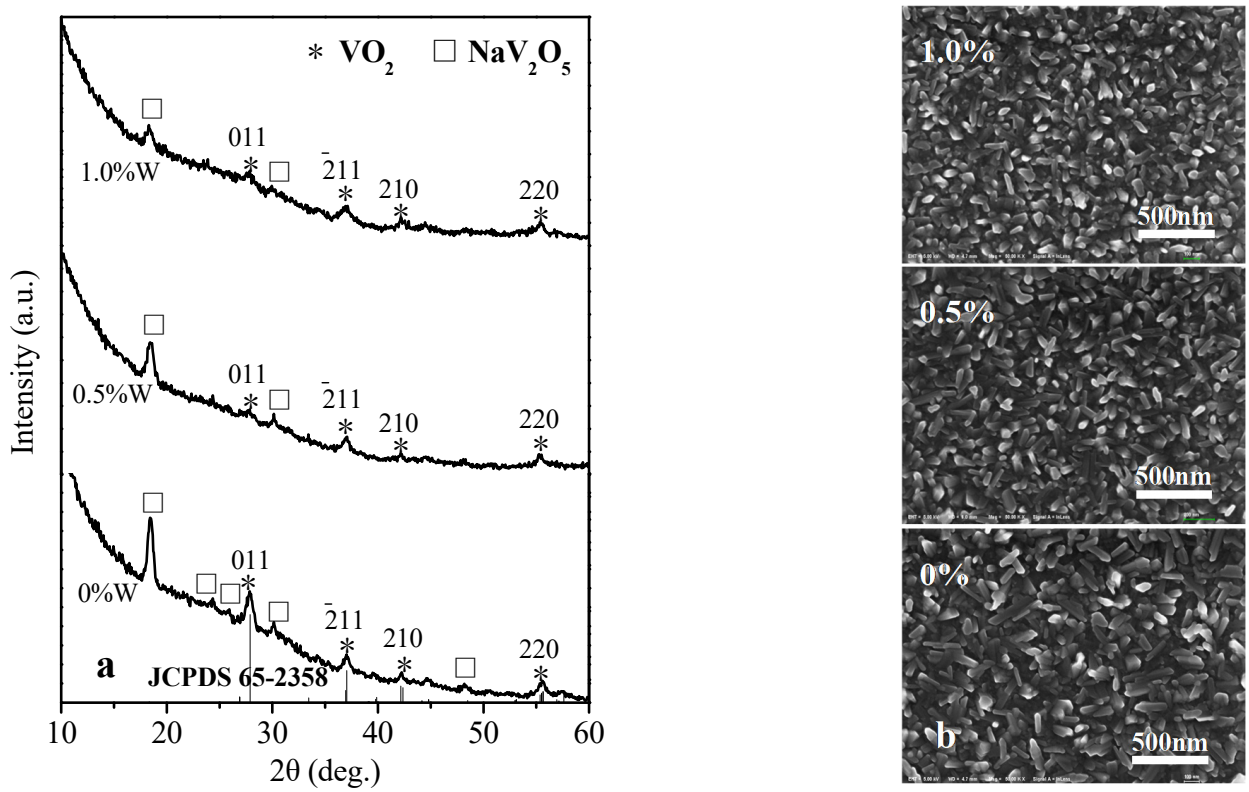

Figure 7. XRD patterns (**a**) and SEM images (**b**) of the W-doped VO_2 thin films prepared by professional annealing of 45 nm W:V films at 450 Pa, 400 °C for 1 h.

3.3. Performance and Micro Morphology of VO_2 Film on Intermediate SiO_2 Layer

The thickness of the intermediate SiO_2 layer prepared by RF magnetron sputtering is approximately 100 nm (Figure 8a). Then, 30 nm V film is deposited on it by DC magnetron sputtering (Table 1). Further, VO_2 films are prepared by professional annealing of the V metal films at 200, 450, and 600 Pa (Table 3). According to the SEM image of the VO_2 film prepared at the optimized pressure 450 Pa (Figure 8c), although the SiO_2 layer is partly punctured, the number of long sheet crystals is significantly reduced. Moreover, it becomes easier to observe the VO_2 crystallites (size about 14 nm by Scherrer Formula) scattering in the film (size about 14 nm too by SEM and software Nano Measurer 1.2.5). Compared with the VO_2 film without SiO_2 layer in Figure 3b-30 nm V, it indicates that the SiO_2 layer plays a crucial role in blocking the diffusion of Na^+ ions, which leads to an increase of the ratio of VO_2: Na-V-O according to the XRD patterns in Figures 3a and 8d, 30 nmV. Consequently, the NIRSE rises (22% at 450 Pa, Figure 8b; original: 20%, Figure 2a), and the near-infrared energy modulation ability $\triangle T_{ir}$ is also enhanced (8.8%; original: 7.0%). Meanwhile, the XRD pattern (Figure 8d) demonstrates that the 100 nm intermediate SiO_2 layer cannot completely prevent the diffusion of Na^+ ions, and a large number of NaV_2O_5 crystals are still generated due to pinholes in the SiO_2 and diffusion of Na through it.

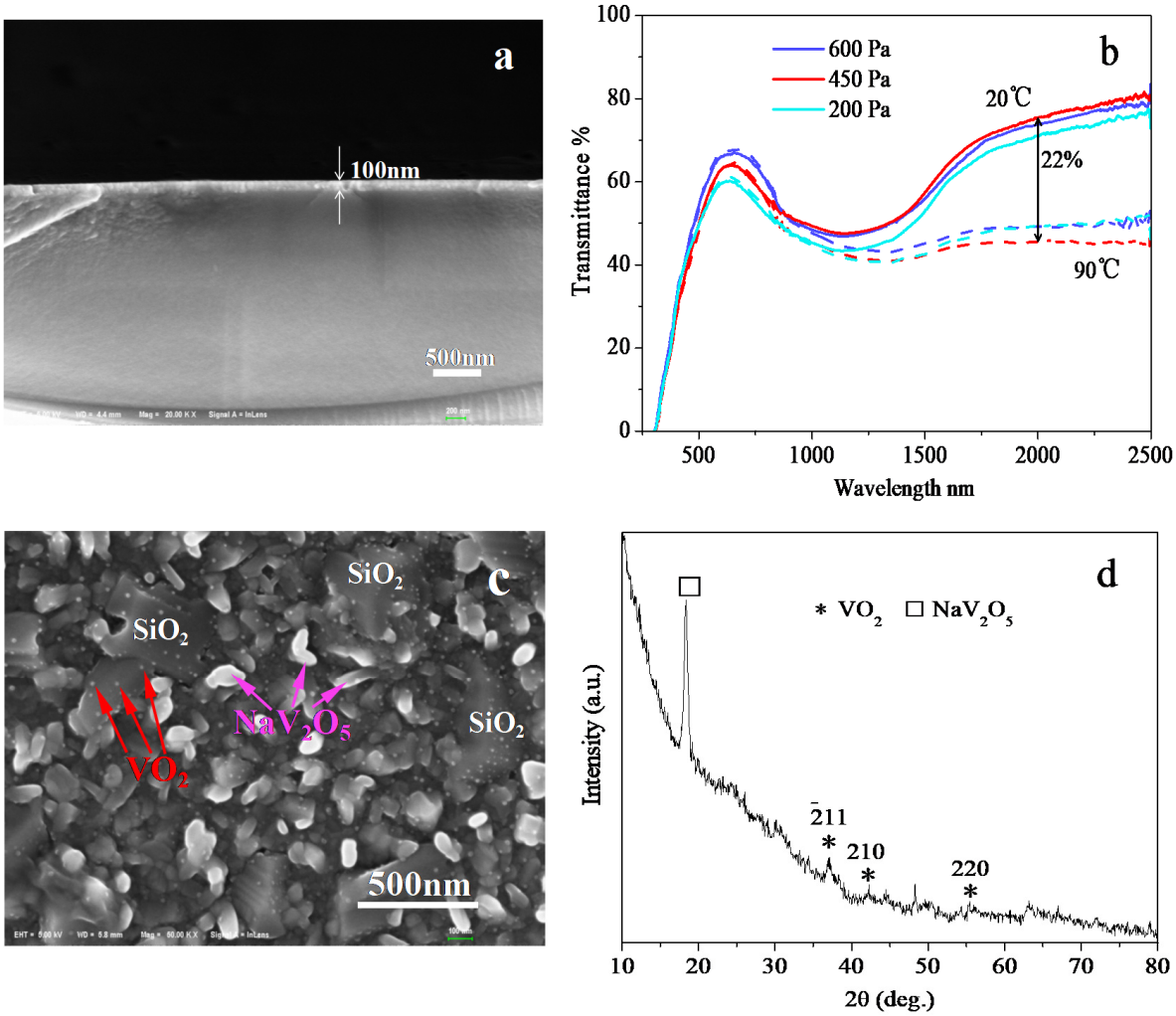

Figure 8. Cross-sectional SEM image of the intermediate SiO_2 layer (**a**); transmittance curves of VO_2 thin films on SiO_2 prepared by professional annealing of 30 nm V at different pressures (**b**); SEM (**c**) and XRD (**d**) patterns of the VO_2 thin film on SiO_2 prepared by professional annealing of 30 nm V at 450 Pa; all at 400 °C for 1 h.

4. Discussion

4.1. Necessity of Two Equipments and Two Steps

The two-step method of magnetron sputtering-professional annealing used in this study not only has good repeatability, but also causes no heat damage to the magnetron sputtering equipment, which can prolong the service life of the equipment. Crystallization using special high-temperature equipment can promote a better phase transition performance. The method can be easily optimized to adjust the doping concentration, oxygen vacancies, content of high-valence NaV_2O_5, film thickness, etc., which are very useful to regulate the phase transition temperature, visible transmittance, and other thermochromic properties.

4.2. Effect of Substrate on the Preparation and Property of VO_2 Thin Film

Generally, the NIRSE of VO_2 film on the glass substrate is lower than that on the quartz glass substrate (Figure 9a). This is because a part of the V atoms react with Na atoms from glass, O atoms from glass, and air to form NaV_2O_5, which results in low production of crystalline VO_2, as shown in the XRD pattern (Figure 9b). In terms of the preparation technique, the VO_2 film prepared on the quartz glass by annealing 30 nm V film at 1500 Pa exhibits a NIRSE value of 50% (Figure 9a). However, the film prepared on the glass by annealing 30 nm V film at 1500 Pa shows a NIRSE value of 0%. Nevertheless,

when the annealing pressure is reduced to 100 Pa, a high NIRSE value (35%, Figure 9a) is achieved. The surface of VO_2 film on quartz glass is flat and compact (Figure 9c), and like a passivation coating, can stand up to the high oxidation pressure 1500 Pa. Meanwhile, the surface of VO_2 film on glass is a loose structure consisted of disordered long sheet NaV_2O_5 crystals and pinholes, which results in greater easiness of oxygen indiffusion from the atmosphere and easiness of oxidization of V to high valence NaV_2O_5 under a high pressure. In addition, there are more free non-bridged oxygen atoms in the glass substrate. Despite the much greater difficulty of O^{2-} ion outdiffusion than Na^+ for its strong Coulomb force, there still is the possibility of O emigrating to the surface and oxidizing the V metal film during the annealing. However, in quartz glass, O atoms are firmly bonded with Si atoms by the covalent bonds and are very difficult to move. So, in conclusion, when on glass substrate, the oxidation pressure is much lower, because of the loose surface of the film majorly, as well as the O outdiffusion from the substrate minorly; and when on quartz glass, the oxidation pressure could be much higher, because of the compact surface of the film.

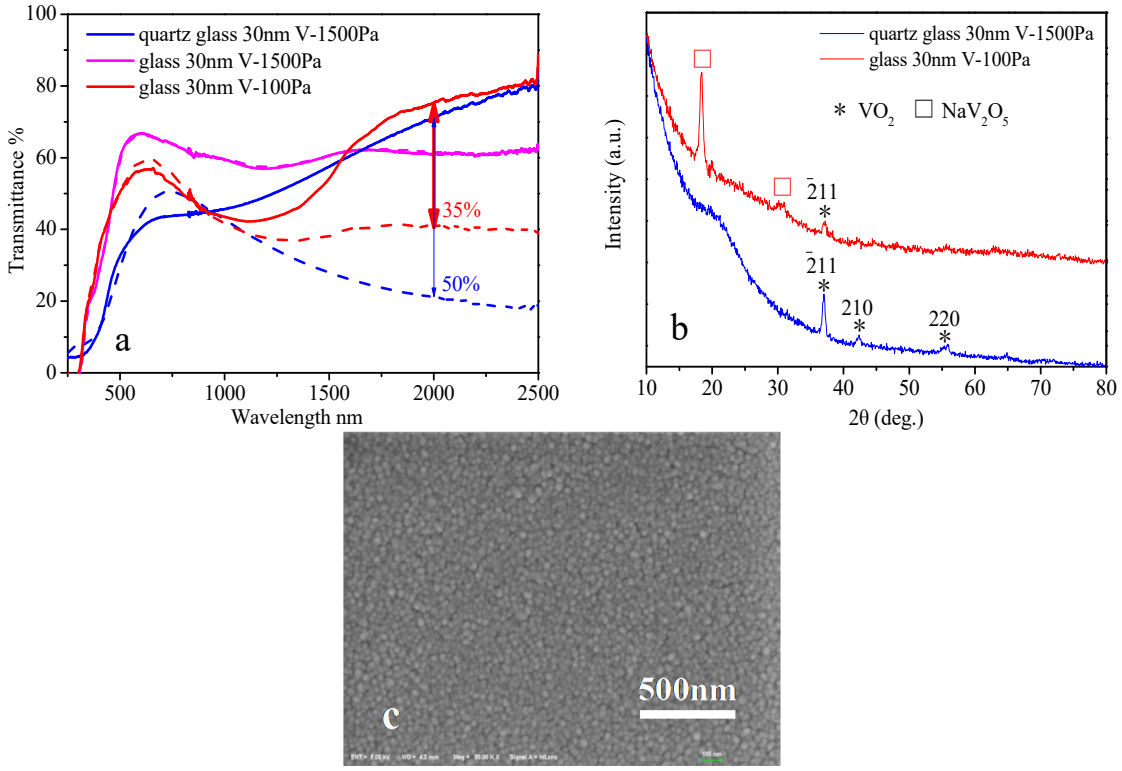

Figure 9. Transmittance curves (solid line: 20 °C, dash line: 90 °C) (**a**), XRD patterns (**b**) of VO_2 films prepared by professional annealing of 30 nm V metal films on two contrastive substrates of quartz glass and float glass at set pressures, 400 °C for 1 h; and SEM image (**c**) of the VO_2 film from "quartz glass 30 nm V-1500 Pa".

4.3. Choice between NIRSE and T_{lum}

The primary goal of VO_2 film preparation is to maximize the value of NIRSE, which means that the content and purity of VO_2 in the film should reach the highest level. However, for smart windows, both NIRSE and visible transmittance T_{lum} should be considered. The minimum daylighting rate of green building glass is generally required to be above 60%. Therefore, it is useful to sacrifice a part of NIRSE to improve the T_{lum}, while ensuring an appropriate high value of NIRSE. The common method to improve the visible transmittance is to deposit anti-reflection films. However, two other simple approaches were used in this study: thinning the V metal film and increasing the annealing pressure. For instance, when the V metal film is thinned from 45 nm to 30 nm, the NIRSE decreases from 39% to 20%, but the T_{lum} increases from 44.5% to 63%, as shown in Figure 2a and

Table 4. When the annealing pressure of 45 nm V film increases from 450 Pa to 700 Pa, the NIRSE decreases from 39% to 30%, but the T_{lum} increases from 44.5% to 61%, as shown in Figure 2b and Table 4. The two methods' mechanism is: at the same high enough oxidation pressure, thinner V metal films will be more easily oxidized into high-valence vanadium; and for the V metal films with same thickness, higher oxidation pressure will result in more high-valence vanadium likewise. The content of low-valence vanadium (mainly crystalline VO_2) in the film decreases, and the content of high-valence vanadium (mainly crystal NaV_2O_5) increases, which leads to an increase in the optical band gap, and results in the increase of the visible transmittance of the film. Moreover, there is another for the thinner film reason, namely lower light absorption.

4.4. Mechanism of W Doping and Equivalent Effect of O Vacancy

There are two mechanisms through which W doping reduces the phase transition temperature (T_c) of VO_2: Peierls mechanism and Mott mechanism. Among them, the Peierls mechanism is described by the energy band theory [34–36], where structural change is considered as the driving force. After larger W atoms replace the smaller V atoms, the lattice expands and the V-V dimerization pairs are destroyed, which results in the change of energy band position. The band gap between V3d$_{//}$and π^* becomes narrower, the electronic migration becomes easier, and the phase transition barrier is reduced, so the T_c decreases. In addition, according to the energy band theory, T_c continues to decline with the increase in the concentration of W dopant, which disagrees with our experimental results (decreases first and then rises). Therefore, this paper supports the second theory of the Mott mechanism. The Mott mechanism is described by the charge-doping theory [37–39], where electron correlation is the driving force. After V^{4+} ions are replaced by W^{6+} ions, the excess electrons enter the empty π^* band, and then local conduction bands and local metallic phases are formed. Therefore, the transformation into tetragonal phase becomes easier, and thus the transition temperature T_c declines. However, excessive W doping can cause superabundant electrons to enter the empty π^* band, and the interaction of electrons is enhanced, which results in the splitting of π^* band and the formation of a new band gap. The phase transition barrier becomes larger, and thus the T_c rises again. The mechanism of W doping to reduce the phase transition temperature of VO_2 is still under debate, just like the debate between Peierls mechanism and Mott mechanism for the intrinsic phase transition of pure VO_2 [40,41]. Presently, there is no unified theory that can fully describe the effect of W doping.

Although the phase transition temperature is reduced by W doping, the thermochromic properties are adversely affected, and the most significant change is that the NIRSE declines significantly. The local conduction bands are formed after W doping, and the electronic transition becomes easier. At low temperature, the ability of reflecting infrared radiation is enhanced, and the infrared transmittance is reduced, and thus the NIRSE is clearly reduced. With the increase of W dopant, the thermal hysteresis loop becomes gentle (Figure 6b) and is no longer steep. This is directly related to the reduction of phase transition temperature at low temperature (below T_d or $T_{d'}$), the rise of phase transition temperature at high temperature (above T_d or $T_{d'}$), and the decline of NIRSE. At low temperature (below T_d or $T_{d'}$), due to the increase of W dopant, local conduction bands in empty π^* band are increased, and the monoclinic-tetragonal phase transition can be easily realized, which results in the reduction of the phase transition temperature. At high temperature (above T_d or $T_{d'}$), due to the gradual increase of tetragonal metallic phase, more and more electrons enter the empty π^* band, and the interaction becomes increasingly stronger, which results in worse fragmentation of the π^* band, a wider band gap, larger phase transition barrier, and thus the increase of the phase transition temperature.

Similar to W doping, the oxygen vacancies can lower the phase transition temperature of VO_2, which were created by lowering the annealing pressure. For example, the T_c of VO_2 film fabricated by annealing 45 nm V film at 200 Pa is 8 °C lower than that of VO_2 film fabricated by annealing 45 nm V film at 450 Pa, as shown in Figure 10a. The oxygen

vacancies lead to the transformation of V^{4+} into V^{3+} and generation of excess electrons, which enter the empty π* band and form a local conduction band. The growth of the charge carrier concentration and the enhancement of the metal phase results in the decline of phase transition temperature, which is similar to the effect of W doping at low concentration. However, it should be noted that when W dopant is used for lowering the phase transition temperature of VO_2, and the concentration has reached an optimal value, i.e., a level (such as 0.5%W) that can cause T_c to rise rather than continually decline, the preparation of oxygen vacancies has an opposite effect. For instance, the T_c of the VO_2 film prepared by annealing 45 nm 0.5%W/V film at 300 Pa is 10 °C higher than that of the VO_2 film prepared by annealing 45 nm 0.5%W/V film at 450 Pa, as shown in Figure 10a. The formation of oxygen vacancies is indicated by the increase of the ratio of V^{3+}: V^{4+} in the $V2p_{3/2}$ XPS spectra (Figure 10b). The three fitting peaks correspond to V^{3+} (515.2 eV), V^{4+} (516.0 eV), and V^{5+} (517.2 eV), respectively [42]. It is found that the V^{3+}: V^{4+} ratio increases from 0.86 to 0.98 when the annealing pressure decreases from 450 Pa to 200 Pa for 45 nm V, and increases from 0.59 to 0.75 when the annealing pressure decreases from 450 Pa to 300 Pa for 45 nm 0.5%W/V.

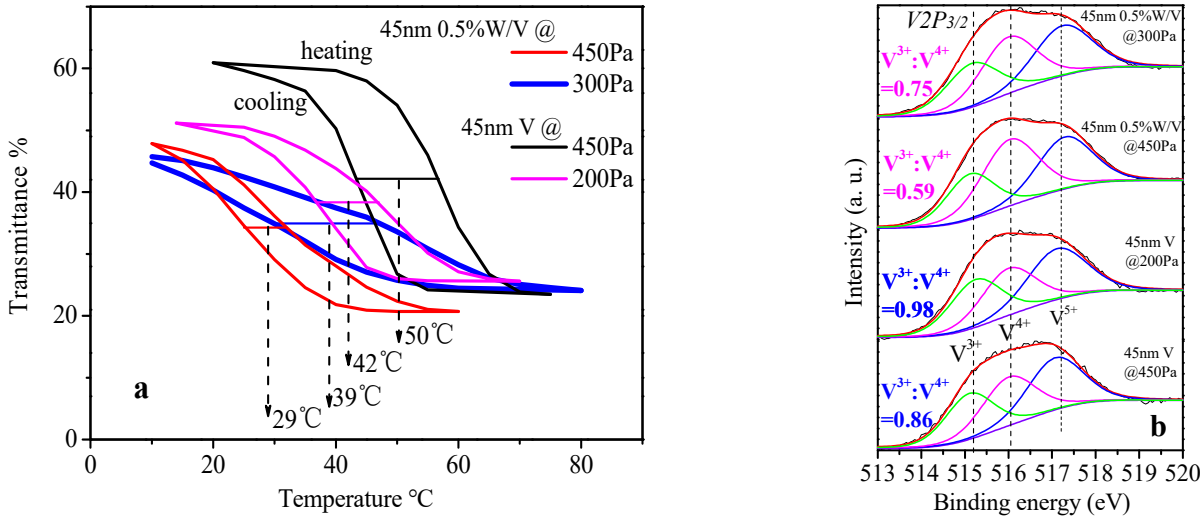

Figure 10. (**a**) Effect of lowering the annealing pressure on the thermal hysteresis loop of the prepared VO_2 films and W/VO_2 films (from 450 Pa to 200 Pa for 45 nm V; from 450 Pa to 300 Pa for 45 nm 0.5%W/V; all at 400 °C for 1 h); (**b**) XPS spectra of V^{3+}, V^{4+} of the corresponding VO_2 films and W/VO_2 films.

In addition, the causes of the decrement of T_c should probably include the strain in the film, as studied by Elia [43], Paez [44], and so on [45]. The substrate used her is glass, so there would not be induction for strain generation by certain lattice planes such as TiO_2(001) [43–45]. However, in spite of this, there would be some strain inevitably existing in the interface between glass and W/VO_2 film, grain boundaries, lattice deformation, and so on. So, the strain in the film after W doping would be another cause for T_c reduction, though not the main cause.

4.5. Effect of 100 nm Intermediate SiO_2 Layer

As described in Section 3.3, a 100-nm-thick intermediate SiO_2 layer pre-deposited on the glass plays an obvious role in blocking the diffusion of Na^+ ions. However, it does not stop the diffusion completely, and many NaV_2O_5 crystals are still generated. As a next step, increasing the thickness of the intermediate SiO_2 layer or replacing it with a better layer (compact, hard, narrow lattice plane, etc.) can completely block the diffusion of Na^+ ions. Meanwhile, the addition of the intermediate SiO_2 layer changes the technical parameters for the preparation of VO_2 thin film, and the optimal oxidation pressure increases from 100 Pa to 450 Pa (Figures 5 and 8b). Similar to the mechanism described in Section 4.2,

the intermediate SiO_2 layer causes fewer long sheet NaV_2O_5 crystals and a flatter, more compact surface than that on glass substrate (Figure 3b-30 nm V, Figure 8c), which results in the difficulty of oxygen indiffusion from the atmosphere. Besides, the intermediate SiO_2 blocks the migration of non-bridged oxygen atoms from the glass into the film. In conclusion, the demand of oxidation annealing pressure rises, mainly because of the compacter surface of the film, and minorly because of the block of O immigration into film from glass.

5. Conclusions

Magnetron sputtering and the professional annealing method have the advantages of simple operation, convenient optimization, good repeatability, and no heat damage to the sputtering machine. Therefore, the represent an appropriate method for the fabrication and systematical examination of VO_2 thin films. To obtain the largest NIRSE value is the primary objective. The thickness must match with the optimal pressure. Otherwise, the value of NIRSE will decline. Under the fixed annealing condition of 400 °C (1 h), a thicker V-based metal film requires a higher optimal annealing pressure, and the thinner film requires a lower optimal annealing pressure. When a glass substrate is used, mainly because of the loose surface structure of disordered long sheet NaV_2O_5 and pinholes, the oxidation annealing pressure reduces sharply. In this study, it was verified that compared with the quartz glass substrate, the annealing pressure of the 30 nm V metal film on the glass substrate decreased by more than 90%. Increasing the annealing pressure or decreasing the thickness of V metal film was demonstrated as a new effective method to improve the visible transmittance T_{lum}. The 100 nm intermediate SiO_2 layer played an obvious role in preventing the diffusion of Na^+ ions, though not completely. Thicker or new intermediate layers need to be further studied. This study supports the charge-doping theory. A proper concentration of W dopant can lead to the formation of local conduction bands in the π^* band, which can reduce the T_c of VO_2 thin film. However, excessive W doping can lead to the splitting of π^* band, which results in the formation of a new band gap and an increase in the phase transition barrier, and thus the T_c increases. In terms of lowering the T_c of VO_2 film, oxygen vacancy and W dopant have an equivalent effect. Further, when the W doping concentration is optimal, no more oxygen vacancies should be added. Otherwise, an opposite effect can occur.

Author Contributions: Conceptualization, X.C. and X.Z. (Xiujian Zhao); methodology, X.C. and Q.X.; software, X.C.; validation, X.C., B.G., X.Z. (Xiaoming Zhang) and J.L.; formal analysis, X.C., Q.X. and X.Z. (Xiujian Zhao); investigation, X.C. and Q.X.; resources, X.C., X.Z. (Xiujian Zhao) and X.Z. (Xiaoming Zhang); data curation, X.C., Q.X. and X.Z. (Xiujian Zhao); writing—original draft preparation, X.C.; writing—review and editing, X.C., X.Z. (Xiaoming Zhang) and X.Z. (Xiujian Zhao); visualization, X.C. and B.G.; supervision, X.Z. (Xiaoming Zhang) and X.Z. (Xiujian Zhao); project administration, X.C. and X.Z. (Xiujian Zhao); funding acquisition, X.C. All authors have read and agreed to the published version of the manuscript.

Funding: This work was supported by the Natural Science Foundation of Jiangxi Province (20202BABL 211011, 20202BABL202012), and Science and Technology Project of Jiangxi Provincial Department of Education (GJJ180860, GJJ190864, GJJ201631).

Institutional Review Board Statement: Not applicable.

Informed Consent Statement: Not applicable.

Data Availability Statement: The data presented in this study are available on request from the corresponding author.

Acknowledgments: The authors would like to thank all the reviewers for their useful comments and suggestions on the manuscript.

Conflicts of Interest: The authors declare no potential conflict of interest with respect to the research, authorship, and/or publication of this article.

References

1. Morin, F.J. Oxides Which Show a Metal-to-Insulator Transition at the Neel Temperature. *Phys. Rev. Lett.* **1959**, *3*, 34–36. [CrossRef]
2. Manousou, D.K.; Gardelis, S.; Calamiotou, M.; Syskakis, E. VO_2 thin films fabricated by reduction of thermal evaporated V_2O_5 under N_2 flow. *Mater. Lett.* **2021**, *299*, 130086. [CrossRef]
3. Yao, T.; Zhang, X.; Sun, Z.; Liu, S.; Huang, Y.; Xie, Y.; Wu, C.; Yuan, X.; Zhang, W.; Wu, Z. Understanding the Nature of the Kinetic Process in a VO_2 Metal-Insulator Transition. *Phys. Rev. Lett.* **2010**, *105*, 226405. [CrossRef] [PubMed]
4. Hu, L.; Tao, H.; Chen, G.; Pan, R.; Wan, M.; Xiong, D.; Zhao, X. Porous W-doped VO_2 films with simultaneously enhanced visible transparency and thermochromic properties. *J. Sol. Gel. Sci. Technol.* **2016**, *77*, 85–93. [CrossRef]
5. Ren, H.; Hassna, O.; Li, J.; Arigong, B. A patterned phase-changing vanadium dioxide film stacking with VO_2 nanoparticle matrix for high performance energy-efficient smart window applications. *Appl. Phys. Lett.* **2021**, *118*, 051901. [CrossRef]
6. Wang, Z.; Li, B.; Tian, S.; Liu, B.; Zhao, X.; Zhou, X.; Tang, G.; Pang, A. Acid Solution Processed VO_2-Based Composite Films with Enhanced Thermochromic Properties for Smart Windows. *Materials* **2021**, *14*, 4927. [CrossRef]
7. Bonora, S.; Beydaghyan, G.; Haché, A.; Ashrit, P. Mid-IR laser beam quality measurement through vanadium dioxide optical switching. *Opt. Lett.* **2013**, *38*, 1554–1556. [CrossRef]
8. Bock, D.C.; Marschilok, A.C.; Takeuchi, K.J.; Takeuchi, E.S. Batteries used to Power Implantable Biomedical Devices. *Electrochim. Acta* **2012**, *84*, 155–164. [CrossRef]
9. Brahlek, M.; Zhang, L.; Lapano, J.; Zhang, H.; Roman, E.; Shukla, N.; Datta, S.; Paik, H.; Schlom, D.G. Opportunities in vanadium-based strongly correlated electron systems. *MRS Commun.* **2017**, *7*, 27–52. [CrossRef]
10. Zhang, C.; Koughia, C.; Güneş, O.; Luo, J.; Hossain, N.; Li, Y.; Cui, X.; Wen, S.; Wong, R.; Yang, Q.; et al. Synthesis, structure and optical properties of high-quality VO_2 thin films grown on silicon, quartz and sapphire substrates by high temperature magnetron sputtering: Properties through the transition temperature. *J. Alloys Compd.* **2020**, *848*, 156323. [CrossRef]
11. Ho, H.; Lai, Y.; Chen, K.; Dao, T.; Nagao, T. High quality thermochromic VO_2 films prepared by magnetron sputtering using V_2O_5 target with in situ annealing. *Appl. Surf. Sci.* **2019**, *495*, 143436. [CrossRef]
12. Rajeswaran, B.; Tadeo, I.J.; Umarji, A.M. IR Photoresponsive VO_2 Thin Films and Electrically Assisted Transition Prepared by Single-Step Chemical Vapor Deposition. *J. Mater. Chem. C* **2020**, *8*, 12543–12550. [CrossRef]
13. Nazari, S.; Charpentier, P.A. Sol-gel processing of VO_2 (M) in supercritical CO_2 and supercritical CO_2/ionic liquid biphasic system. *J. Supercrit. Fluids* **2020**, *165*, 104989. [CrossRef]
14. Bukhar, S.A.; Kumar, S.; Kumar, P.; Gumfekar, S.P.; Chung, H.J.; Thundat, T.; Goswami, A. The effect of oxygen flow rate on metal–insulator transition (MIT) characteristics of vanadium dioxide (VO_2) thin films by pulsed laser deposition (PLD). *Appl. Surf. Sci.* **2020**, *529*, 146995. [CrossRef]
15. Zhang, D.; Sun, H.; Wang, M.; Miao, L.; Liu, H.; Zhang, Y.; Bian, J. VO_2 Thermochromic Films on Quartz Glass Substrate Grown by RF-Plasma-Assisted Oxide Molecular Beam Epitaxy. *Materials* **2017**, *10*, 314. [CrossRef]
16. Gurvitch, M.; Luryi, S.; Polyakov, A.; Shabalov, A.; Dudley, M.; Wang, G.; Ge, S.; Yakovlev, V. VO_2 films with strong semiconductor to metal phase transition prepared by the precursor oxidation process. *J. Appl. Phys.* **2007**, *102*, 033504. [CrossRef]
17. Luo, Z.; Wu, Z.; Xu, X.; Wang, T.; Jiang, Y. Study of nanocrystalline VO_2 thin films prepared by magnetron sputtering and post-oxidation. *Chin. Phys. B* **2010**, *19*, 106103.
18. Liu, X.; Wang, S.; Chen, F.; Yu, L.; Chen, X. Tuning phase transition temperature of VO_2 thin films by annealing atmosphere. *J. Phys. D-Appl. Phys.* **2015**, *48*, 5104–5111. [CrossRef]
19. Xu, X.; Yin, A.; Du, X.; Wang, J.; Liu, J.; He, X.; Liu, X.; Huan, Y. A novel sputtering oxidation coupling (SOC) method to fabricate VO_2 thin film. *Appl. Surf. Sci.* **2010**, *256*, 2750–2753. [CrossRef]
20. Ba, C.; Fortin, V.; Bah, S.T.; Pandurang, R.V. Formation of VO_2 by rapid thermal annealing and cooling of sputtered vanadium thin films. *J. Vac. Sci. Technol. A* **2016**, *34*, 031505. [CrossRef]
21. Lust, M.; Chen, S.; Wilson, C.E.; Argo, J.; Ghalichechian, N. High-contrast, highly textured VO_2 thin films integrated on silicon substrates using annealed Al_2O_3 buffer layers. *J. Appl. Phys.* **2020**, *127*, 205303. [CrossRef]
22. Lin, T.; Zhang, Y.; Zheng, D. The ultrathin VO_2 (M) film with ultrahigh visible transmittance synthesized on the quartz glass substrate by HiPIMS. *Vacuum* **2018**, *156*, 449–455. [CrossRef]
23. Cesca, T.; Scian, C.; Petronijevic, E.; Leahu, G.; Mattei, G. Correlation between in situ structural and optical characterization of the semiconductor-to-metal phase transition of VO_2 thin films on sapphire. *Nanoscale* **2019**, *12*, 851–863. [CrossRef] [PubMed]
24. Miller, M.J.; Wang, J. Influence of Na diffusion on thermochromism of vanadium oxide films and suppression through mixed-alkali effect. *Mater. Sci. Eng. B* **2015**, *200*, 50–58. [CrossRef]
25. Abbott, D.; Janjan, B.; Miri, M.; Fathi, D.; Heidari, M. Hybrid Si_3N_4/VO_2 Modulator Thermally Triggered by a Graphene Microheater. *IEEE J. Sel. Top. Quantum Electron.* **2020**, *26*, 1–7.
26. Kang, C.; Zhang, C.; Zhang, L.; Liang, S.; Geng, C.; Cao, G.; Zong, H.; Li, M. Transformation of crystalline structure and photoelectric properties in VO_2/glass thin films by inserting TiO_2 buffer layers. *Appl. Surf. Sci.* **2019**, *463*, 704–712. [CrossRef]
27. Chu, X.; Tao, H.; Liu, Y.; Ni, J.; Bao, J.; Zhao, X. VO_2/AZO double-layer films with thermochromism and low-emissivity for smart window applications. *J. Non-Cryst. Solids* **2014**, *383*, 121–125. [CrossRef]
28. Zhu, B.; Tao, H.; Zhao, X. Effect of buffer layer on thermochromic performances of VO_2 films fabricated by magnetron sputtering. *Infrared Phys. Technol.* **2016**, *75*, 22–25. [CrossRef]

29. Victor, J.L.; Marcel, C.; Sauques, L.; Labrugere, C.; Amiard, F.; Gibaud, A.; Rougier, A. From multilayers to $V_{1-x}W_xO_{2\pm\delta}$ films elaborated by magnetron sputtering for decreasing thermochromic transition temperature. *J. Alloys Compd.* **2020**, *858*, 157658. [CrossRef]
30. Lee, J.S.; Shibuya, K.; Kawasaki, M.; Tokura, Y. Optical investigation of metal-insulator transitions in $V_{1-x}W_xO_2$ ($0 \leq x \leq 0.33$). *Phys. Rev. B* **2012**, *85*, 155110.1–155110.5. [CrossRef]
31. Fan, L.; Wang, X.; Wang, F.; Zhang, Q.; Zhu, L.; Meng, Q.; Wang, B.; Zhang, Z.; Zou, C. Revealing the role of oxygen vacancies on the phase transition of VO_2 film from the optical-constant measurements. *RSC Adv.* **2018**, *8*, 19151–19156. [CrossRef]
32. *ISO 9050-2003*; Glass in Building-Determination of Light Transmittance, Solar Direct Transmittance, Total Solar Energy Transmittance, Ultraviolet Transmittance and Related Glazing Factors. International Organization for Standardization: Geneva, Switzerland, 2003.
33. Mjejri, I.; Etteyeb, N.; Sediri, F. NaV_2O_5 nanoplates: Hydrothermal synthesis, characterization and study of their optical and electrochemical properties. *Ceram. Int.* **2014**, *40*, 5379–5386. [CrossRef]
34. Miao, L.; Peng, Y.; Wang, D.; Liang, J.; Hu, C.; Nishibori, E.; Sun, L.; Fisher, C.A.; Tanemura, S. Characterisation of the temperature-dependent M1 to R phase transition in W-doped VO_2 nanorod aggregates by Rietveld refinement and theoretical modelling. *Phys. Chem. Chem. Phys.* **2020**, *22*, 7984–7994. [CrossRef] [PubMed]
35. Booth, J.M.; Casey, P.S. Anisotropic Structure Deformation in the VO_2 Metal-Insulator Transition. *Phys. Rev. Lett.* **2009**, *103*, 086402. [CrossRef] [PubMed]
36. Goodenough, J.B. The two components of the crystallographic transition in VO_2. *J. Solid State Chem.* **1971**, *3*, 490–500. [CrossRef]
37. Zhou, J.; Xie, M.; Cui, A.; Zhou, B.; Jiang, K.; Shang, L.; Hu, Z.; Chu, J. Manipulating Behaviors from Heavy Tungsten Doping on Interband Electronic Transition and Orbital Structure Variation of Vanadium Dioxide Films. *ACS Appl. Mater. Interfaces* **2018**, *10*, 30548–30557. [CrossRef]
38. Talcami, H.; Kanki, T.; Ueda, S.; Kobayashi, K.; Tanaka, H. Filling-controlled molt transition in W-doped VO_2. *Phys. Rev. B* **2012**, *85*, 45–51.
39. Sakai, E.; Yoshimatsu, K.; Shibuya, K.; Kumigashira, H.; Ikenaga, E.; Kawasaki, M.; Tokura, Y.; Oshima, M. Competition between instabilities of Peierls transition and Mott transition in W-doped VO_2 thin films. *Phys. Rev. B* **2011**, *84*, 195132. [CrossRef]
40. Quackenbush, N.F.; Paik, H.; Holtz, M.E.; Wahila, M.J.; Moyer, J.A.; Barthel, S.; Wehling, T.O.; Arena, D.A.; Woicik, J.C.; Muller, D.A. Reducing orbital occupancy in VO_2 suppresses Mott physics while Peierls distortions persist. *Phys. Rev. B* **2017**, *96*, 081103.1–081103.5. [CrossRef]
41. Ling, C.; Wang, Q.; Wang, X.; Zhao, Z.; Wang, Z.; Li, J.; Zhao, Y.; Jin, H. Hole Dopants Disentangling Peierls–Mott Relevance States of VO_2 by First-Principles Calculation. *J. Phys. Chem. C* **2021**, *125*, 5816–5823. [CrossRef]
42. Geert, S.; Diederik, D.; Hilde, P.; Guy, B.M.; Roger, D.G. Determination of the V2p XPS binding energies for different vanadium oxidation states (V^{5+} to V^{0+}). *J. Electron Spectrosc. Relat. Phenom.* **2004**, *135*, 167–175.
43. D'Elia, A.; Grazioli, C.; Cossaro, A.; Li, B.W.; Zou, C.W.; Rezvani, S.J.; Pinto, N.; Marcelli, A.; Coreno, M. Strain mediated filling control nature of the metal-insulator transition of VO_2 and electron correlation effects in nanostructured films. *Appl. Surf. Sci.* **2021**, *540*, 148341. [CrossRef]
44. Paez, G.J.; Singh, C.N.; Wahila, M.J.; Tirpak, K. Simultaneous Structural and Electronic Transitions in Epitaxial VO_2/TiO_2 (001). *Phys. Rev. Lett.* **2020**, *124*, 196402. [CrossRef] [PubMed]
45. Muraoka, Y.; Hiroi, Z. Metal-insulator transition of VO_2 thin films grown on TiO_2 (001) and (110) substrates. *Appl. Phys. Lett.* **2002**, *80*, 583. [CrossRef]